Applied Energy 105 (2013) 335–348

Contents lists available at SciVerse ScienceDirect

Applied Energy

journal homepage: www.elsevier.com/locate/apenergy

# Fuel economy optimization of an Atkinson cycle engine using genetic algorithm

Jinxing Zhao, Min Xu *

*National Engineering Laboratory for the Automotive Electronic Control Technology, Shanghai Jiao Tong University, 800 Dongchuan Rd., Shanghai 200240, China*

## HIGHLIGHTS

- A 1-D engine simulation model that covers entire speed–load operating range is built.
- The engine model is carefully calibrated using experimental data.
- Optimization methodology based on the 1-D engine simulation model is proposed.
- Part load operating variables are automatically optimized using the method.
- Significant fuel economy improvement is obtained after optimized by genetic algorithm.

## ARTICLE INFO

*Article history:*
Received 15 October 2012
Received in revised form 22 December 2012
Accepted 26 December 2012
Available online 9 February 2013

*Keywords:*
Atkinson cycle engine
Fuel economy
Genetic algorithm
Part load modeling
Model based optimization
Calibration

## ABSTRACT

An Atkinson cycle engine with geometrical compression ratio (GCR) of 12.5 has been designed by maximizing fuel economy at full load operating conditions based on the Artificial Neural Network Method [1]. However, the Atkinson cycle engine generally operates at part load conditions especially in the middle to high load range. Optimization of the fuel economy for part load is more important in reducing the total fuel consumption. The Atkinson cycle engine applies the load control strategy that combines the intake valve closure (IVC) timing and electrically throttling control (ETC), which has an impact to the fuel economy. Moreover, the exhaust valve opening (EVO) timing, spark angle (SA) and air–fuel-ratio (AFR) also affect the fuel economy. If calibrating these operating variables over the entire operating range through experiments, the difficulty and cost will become a big issue. A physical model based optimization scheme by coupling MATLAB genetic algorithm (GA) and 1-D GT-Power simulation models of the Atkinson cycle engine are proposed. The GT-Power models were improved to accurately simulate the part load conditions, by calibrating parameters of the combustion and heat transfer sub-models using experimental data taken at various speed–load points covering the entire operating range. The fuel economy was optimized based on the part-load calibrated GT-Power models using the Genetic Algorithm. After each speed–load point was optimized, the control maps for the IVC timings, SA, etc. were obtained. Then these numerically optimized control maps were input into the engine control unit (ECU) as the initial values of the engine calibration, which were further experimentally optimized. The experimental results show that the part-load GT-Power models have sufficient prediction accuracy, with maximal error of 8.5%. After optimized by GA, the fuel economy was greatly improved over the operating range, with the maximal improvement up to 7.67%.



## 1. Introduction

An Atkinson cycle engine (Appendix 1) with geometrical compression ratio of 12.5 has been designed and built [1]. Fuel economy at widely-open-throttle (WOT) operating conditions in the speed range from 1000 rpm to 4400 rpm of the Atkinson cycle engine are greatly improved comparing to its baseline Otto cycle engine. The maximum improvement is up to 13% at 2400 rpm.

However, the Atkinson cycle engine mainly works at part load operating conditions especially in the middle to high load range when it is used in a hybrid vehicle [2]. In the hybrid system, an Atkinson cycle engine could always work in the highly efficient operating conditions at any time through optimum collaborative control of an engine, a motor, a generator via a power split device [2–4]. The fuel economy for the Atkinson cycle engine at part load (not WOT) operating conditions are more important and useful for practical fuel consumption reduction.

The Atkinson cycle engine applies the load control strategy that combines the intake valve closure (IVC) timing and electrically

* Corresponding author. Tel.: +86 21 3420 6670.
*E-mail address:* mxu@sjtu.edu.cn (M. Xu).

0306-2619/$ - see front matter © 2012 Elsevier Ltd. All rights reserved.
http://dx.doi.org/10.1016/j.apenergy.2012.12.061

**Nomenclature**

| | |
|---|---|
| $m_e$ | entrained mass of the unburned mixture |
| $\rho_u$ | unburned mixture density at time of spark |
| $A_f$ | entrainment surface area at the edge of the flame front |
| $\mu_T$ | characteristic speed related with the turbulent intensity |
| $S_L$ | laminar flame speed |
| $m_b$ | burned mass |
| $\tau_b$ | characteristic burning time |
| $l_M$ | Taylor micro-scale length; |
| $\mu$ | parametric mass (interpreted as the mass entrained within the flame region that has yet to burn) |
| $B_m$ | maximum laminar speed |
| $B_\phi$ | laminar speed roll-off value |
| $\phi$ | in-cylinder equivalence ratio |
| $\phi_m$ | equiv. ratio at max. speed |
| $T_u$ | temperature of the unburned gas |
| $R_f$ | mass fraction of the residuals in the unburned zone |
| $A$ | temperature ratio exponent |
| $B$ | pressure ratio exponent |
| $DEM$ | dilution exponent multiplier |
| $m_1$ | flame kernel growth multiplier |
| $m_2$ | turbulent Flame Speed Multiplier |
| $m_3$ | Taylor length scale multiplier |
| $m_4$ | convection multiplier |
| $\mu_T$ | characteristic speed is closely related with in-cylinder turbulence intensity |
| $\bar{u}_i$ | mean inlet gas speed |
| $\eta_v$ | volumetric efficiency |
| $A_p$ | piston area |
| $a_{iv}$ | the maximum open area of the inlet valve |
| $\bar{S}_p$ | the mean piston speed |
| $\dot{q}$ | heat flux |
| $T_w$ | wall temperature |
| $A_w$ | wall surface area in contact with the cylinder gases |
| $B$ | the cylinder bore |
| $h_c$ | the heat-transfer coefficient |
| $w$ | average cylinder gas velocity |
| $p$ | average cylinder gas pressure |
| $T$ | average cylinder gas temperature |
| HRR | apparent heat release rate |
| AFR | air–fuel-ratio |
| ETC | electrically throttle control valve |
| IVC | intake valve closure |
| EVO | exhaust valve open |
| SA | spark angle |

throttling control (ETC), whose operating parameters are different from those of the traditional Otto cycle engine. In order to realize the Atkinson cycle at partial loads, the late-intake-valve-closing (LIVC) operation could be adopted to shorten the effective compression stroke. On the one hand, the LIVC operation may cause a backflow of the fresh charge during the early compression stroke if it is too late. Due to the LIVC effect, at a specific load level, a lighter throttling operation is usually required which also reduces the pumping loss [5–8]. The LIVC operation reduces effective compression ratio and results in lower mixture temperature at the end of compression stroke. The lower mixture temperature reduces the initial combustion velocity and increases the 0–50% combustion duration, hence degrades the cycle thermal efficiency [5,9]. On the other hand, the minimum best torque (MBT) spark timing can be advanced due to lower charge temperature, which enlarge the constant volume combustion portion thus improves the thermal efficiency slightly [9]. Therefore, the LIVC operation has conflicting effects on the thermal efficiency for the Atkinson cycle engine. Moreover, the exhaust valve open (EVO) timing and air–fuel-ratio (AFR) also have significant effects on the fuel economy of the engine.

The LIVC operation and other operating variables are highly interdependent and have different effects on the fuel economy of the Atkinson cycle engine, which will make the optimization and calibration very time-consuming and expensive. Recently, some model based calibration methods and tools have been developed to conduct the optimization and calibration works for the engine operating variables [10–15]. Guerrier and Cawsey [10] and Carter and Gabler [11] introduced application examples of the Model Based Calibration (MBC) toolbox in MATLAB software. The MBC method firstly established the objective mathematic models based on numerical method (such as the polynomial fitting) using experimental or simulation data. Then the optimization works were done based on the mathematic models. Wu B. used artificial neural network technique to build the surrogate models of the 1-D simulation software in order to optimize the cam phasing to maximize the torque output at WOT operating conditions [12] and to improve the fuel economy and reduce NOx emissions at part loads [13]. Togun and Baysec [14] used the artificial neural networks to model the torque and specific fuel consumption of a gasoline engine. D'Errico et al. [15] defined an efficient methodology for the internal combustion engine (ICE) design and optimization based on a 1D fluid dynamic physical model. The direct search algorithm and Genetic Algorithm (GA) were chosen and compared to solve single- and multi-objective optimization problems.

Classical numerical optimization methods are only applicable to continuously differentiable functions. Moreover, those methods are easy to drop in local minima and their performances depend on the chosen initial values. Fortunately, the GA is more suitable for the systems that are complex, highly nonlinear and not obvious analytical such as the engine system addressed in this paper. Furthermore, the GA is less likely to get trapped in local minima, and is not restricted by continuity or differentiability requirements on the objective functions. Therefore, the GA was used as the optimization technique in our optimization work.

In recent years, GA has been widely used in the engine field to perform optimization of the design and operating variables [16–20] or to identify engine model parameters [21]. Alonso et al. [16] used artificial neural network (ANN) to model the experimental emission data of a diesel engine, then the operating variables were optimized based on the ANN models and GA to reduce the emissions. Hiroyasu et al. [17] applied the multi-objective genetic algorithm (MOGA) to optimize EGR, injection timing and other relevant operating variables to improve the fuel efficiency and reduce the emissions. Verma and Lakshminarayanan [18] used GA to optimize the injection timing of a diesel engine to improve the fuel economy while meeting the NOx emission limit, which illustrates the adaptability of GA on complex optimization problems. Vossoughi and Rezazade [19] demonstrated the capability of MOGA in the calibrations of the engine management system (EMS) based on ANN modeling method. Lampinen [20] developed a GA based computer aided design methodology to implement automatic design and optimization of complex problems. The cam shapes were described by a computer program. The proposed method is more efficient and accurate than the conventional method using experiences and trial and errors. Li and Pilidis [21] investigated a GA based gas turbine design-point performance adaptation approach to best estimate the unknown component parameters and optimize engine performance.

However, there has not been any published investigation about directly using engine physical model to conduct the engine calibrations over the entire speed–load operating range. The method in Refs. [10–13,16–19] must first build the numerical optimization model using simulation or experimental data. If only using experimental data that cover all speed–load points to build the mathematic model for complex engine system, the experimental tasks would be huge and the associated cost will be too large to be acceptable. D'Errico et al. [15] carried out an ICE design and optimization based on 1-D dynamic physical models. However, they only validated the model at full load, but used the model to do optimization works for part loads without any validation. Thus the model accuracy should be doubted. Therefore, to realize the physical model based automatic calibration of operating parameters, the accurate enough 1-D engine models over the entire engine operating range including part loads are in the critical path.

A model based optimization methodology, which was realized by coupling MATLAB GA and the part-load calibrated 1-D GT-Power physical models of the Atkinson cycle engine, is proposed in this paper. The 1-D simulation models were carefully calibrated by using experimental data at several representative speed–load points that cover the entire engine speed–load range. Basing on the 1-D physical models, the operating variables (IVC timing, etc.) can be further optimized by GA to improve the fuel economy. The optimization results (control maps) for the operating variables at each load level of each speed were computed by the proposed optimization methodology. Then, these computed control maps were applied to experimentally calibrate the engine control unit (ECU). Those operating variables were further experimentally optimized to obtain the maximum fuel economy at each operating point.

## 2. The engine model

### 2.1. The Atkinson cycle engine

Table 1 lists the main specifications of the Atkinson cycle engine. This Atkinson cycle engine was developed based on a 1.8L double VVT Otto cycle engine with geometrical compression ratio (GCR) of 10.6. The GCR 12.5 of the Atkinson cycle engine was realized by increasing the medium height of the piston to reduce the combustion chamber volume [1].

The vane operating angle range for both intake and exhaust VVT device is 40CA. The initial intake valve variable range for the Otto cycle engine is 70–110CA after bottom dead center (ABDC). Considering the bigger GCR for the Atkinson cycle engine and the LIVC operation, as well as the combined load control effects of the intake VVT device and the throttling body at part load operating conditions, the variable range of the intake VVT for the Atkinson cycle engine was retarded 5CA compared to the Otto cycle engine.

### 2.2. GT-Power model of the Atkinson cycle engine

Fig. 1 shows the schematic of the 1D GT-Power model of the Atkinson cycle engine. The GT-Power model of the baseline Otto cycle engine at WOT operating conditions have been built and carefully calibrated in Ref. [1]. However, this model can only be used to simulate the WOT operating conditions. For the part load conditions, the combustion and heat-transfer related sub-models need to be re-built and re-calibrated using the part load experimental data.

**Table 1**
Main engine specifications.

| | |
|---|---|
| Total displacement ($cm^3$) | 1799 |
| Cylinder/valve number (−) | 4/16 |
| Bore (mm) | 80 |
| Stroke (mm) | 89 |
| Length of connection rod (mm) | 133.1 |
| Geometrical compression ratio (−) | 12.5 |
| Fuel injection type (−) | MPI |
| VVT operating range (CA) | 40 |
| IVC (CA ABDC) | 75–115 |
| EVO (CAATDC) | 90–130 |

The two-zone quasi 3-D turbulent flame combustion model, namely SITurb [22], is used to predict the apparent heat release rate (HRR). It can take into account the effects of dilutions (e.g., residual gases) and the mixture temperature on the HRR. Hence, the influences of VVT and AFR on the HRR could be simulated using this combustion model.

The Woschni model [22,23] is adopted to simulate all heat-transfer processes. Mathematical expressions of the basic SITurb combustion model [22,23] and Woschni heat-transfer model [23] are shown in the Table 2.

Eqs. (1)–(6) in Table 2 describe the original SI engine combustion model derived by Keck and his coworkers [23]. Eq. (1) describes the burning rate of mixture. The first term on the right side represents the laminar (diffusive) propagation of the flame front, which is determined by the laminar flame speed ($S_L$ in Eq. (6)) and mixture density. The second term represents the burning rate of mixture already entrained within this flame front, which is related to turbulent velocity ($\mu_T$ in Eq. (3)). Eq. (2) describes the rate of change of unburned mixture mass $\mu$ within the flame zone. The first term represents the turbulent convection of unburned mixture across the flame front, and the second term represents the mass rate of the burning mixture that is still contained within the flame zone. The exponential term in the brackets describes the fact that the flame sheet initially is spherical and laminar-like: it requires a time of about $\tau_b$ (characteristic burning time in Eq. (5)) to develop into a turbulent flame.

It can be found in Eq. (1) that the burning rate of mixture is mainly determined by unburned mixture density, laminar flame speed, unburned mixture mass within the flame zone, turbulent velocity and characteristic burning time. When these values are calculated, the burning rate of mixture could be calculated by substituting these values into Eq. (1).

The Woschni heat-transfer sub-model is mainly used to describe the steady-flow forced-convection heat-transfer problems, in which the heat flux $\dot{q}$ transferred to a solid surface at temperature $T_w$ from a flowing fluid stream at temperature $T$ is determined from the Eq. (14).

The burning rate of mixture together with the heat-transfer loss determines the in-cylinder pressure and the final performance of the engine. At each speed–load point, you can obtain accurate burning rate and heat-transfer loss by carefully adjusting the relevant terms in Eqs. (1–6 and 14 and 15). For example, the burning rate of a specific speed–load point could be adjusted by changing the turbulent velocity in Eq. (2). In this way, accurate burning rate and heat loss of all speed–load points could be obtained and final engine performances could be accurately predicted.

The SI engine combustion model (Eqs. (1) and (2)) is empirically based, and derived based on coupled analysis of flame front location and cylinder pressure data at several sets of engine operating conditions. Additionally, the $u_T$ in Eq. (3) is also empirical correlation derived by applying Eqs. (1) and (2) to several sets of engine combustion data [23].

Similar to the combustion model, the Woschni heat-transfer model is also a data-derived model obtained by fitting the heat-transfer data under a wide range of engine operating conditions.

Therefore, the SITurb and Woschni are all phenomenological and data-derived empirical models. The two models were derived based on the experimental data of some typical engine operating conditions. Therefore, once the simulated operating condition changes, the relevant model parameters in the two models must

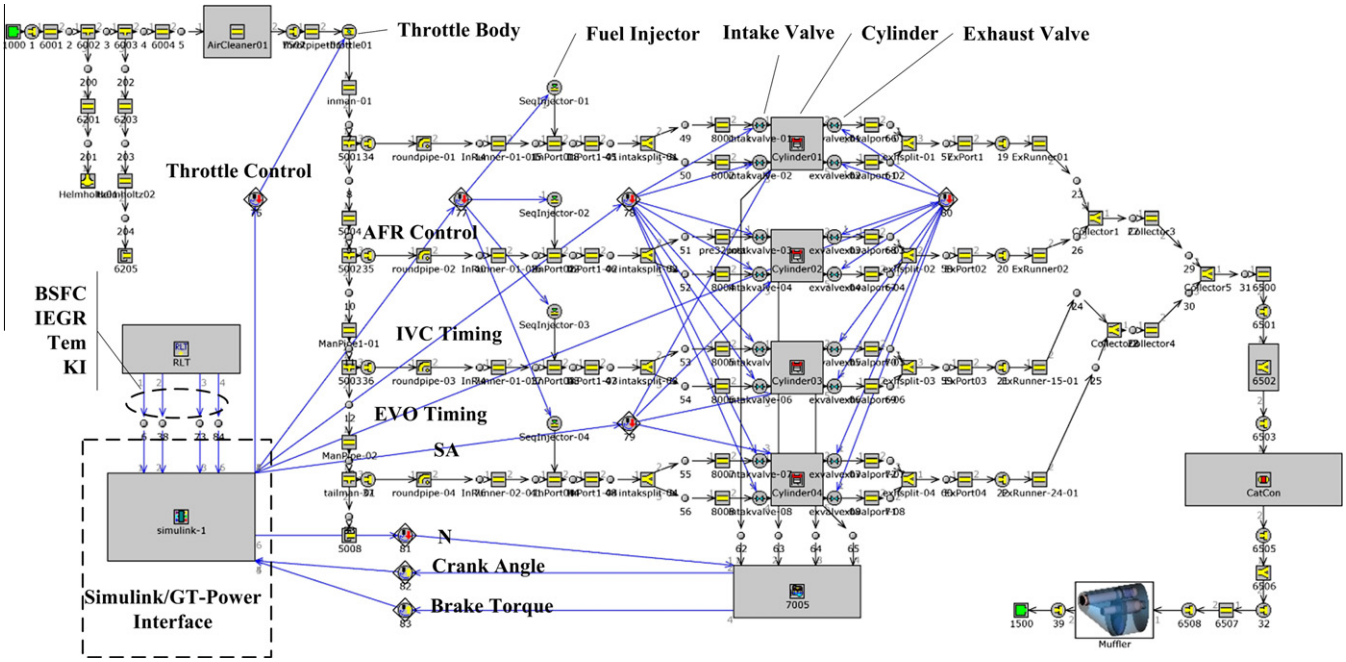


**Fig. 1.** GT-Power model of the Atkinson cycle engine.

**Table 2**
SITurb combustion model and Woschni heat-transfer model.

| Basic model | | Modified model | |
|---|---|---|---|
| SITurb : $\frac{dm_b}{dt} = \rho_u A_f S_L + \frac{\mu}{\tau_b}$ | (1) | SITurb : $\frac{dm_b}{dt} = \rho_u A_f S_L^* + \frac{\mu}{\tau_b^*}$ | (7) |
| $\frac{d\mu}{dt} = \rho_u A_f u_T (1 - e^{-t/\tau_b}) - \frac{\mu}{\tau_b}$ | (2) | $\frac{d\mu}{dt} = \rho_u A_f u_T^* (1 - e^{-t/\tau_b^*}) - \frac{\mu}{\tau_b^*}$ | (8) |
| $u_T = 0.08 \bar{u}_i \left(\frac{\rho_u}{\rho_i}\right)^{1/2}$ | (3) | $u_T^* = m_2 0.08 \bar{u}_i \left(\frac{\rho_u}{\rho_i}\right)^{1/2}$ | (9) |
| $\mu = m_e - m_b$ | (4) | $\mu = m_e - m_b$ | (10) |
| $\tau_b = \frac{l_M}{S_L}$ | (5) | $\tau_b^* = \frac{l_M^*}{S_L^*}$ | (11) |
| $S_L = (B_m + B_\phi(\phi - \phi_m)^2) * \left[\frac{T_u}{T_{ref}}\right]^\alpha \left[\frac{p}{p_{ref}}\right]^\beta (1 - 2.06 R_f^{0.77DEM})$ | (6) | $S_L^* = m_1 S_L$ | (12) |
| | | $l_M^* = m_3 l_M$ | (13) |
| Woschni : $\dot{q} = A_w h_c (T - T_w)$ | (14) | Woschni : $\dot{q}^* = m_4 A_w h_c (T - T_w)$ | (16) |
| $h_c = 3.26 B^{-0.2} p^{0.8} T^{-0.55} w^{0.8}$ | (15) | $h_c = 3.26 B^{-0.2} p^{0.8} T^{-0.55} w^{0.8}$ | (17) |

be accordingly modified and calibrated using the experimental data taken at the same operating condition to correctly predict the HRR and heat loss at this condition. Otherwise, the engine performances predicted by the GT-Power model will have significant error.

The following parameters were introduced to modify the SITurb and Woschni sub-models in order to simulate the part load operating conditions, and they were calibrated at various speeds and loads to cover the entire engine speed and load range: *Dilution Exponent Multiplier* (the *DEM* in Eq. (6)), *Flame Kernel Growth Multiplier, Turbulent Flame Speed Multiplier* and *Taylor Length Scale Multiplier* in the SITurb sub-model, and *Convection Multiplier* in the Woschni sub-model.

The Flame Kernel Growth Multiplier, Turbulent Flame Speed Multiplier, Taylor Length Scale Multiplier and Convection Multiplier are denoted by $m_1$, $m_2$, $m_3$ and $m_4$, respectively.

*DEM* needs to be calibrated to consider the effect of in-cylinder residual on the laminar flame speed in Eq. (6). Increasing this value will reduce the effect of residual dilution on the laminar flame speed. In the GT-Power model, this parameter was only calibrated to vary with load, which is due to the reality that the in-cylinder residual fraction varies significantly with load but not obviously with engine speed.

$m_1$: needs to be calibrated to scale the growth rate of the flame kernel. This parameter scales the laminar flame speed in Eq. (6) thus the characteristic burning time $\tau_b$ in Eq. (5). Increasing this value will advance the transition from the laminar combustion to the turbulent combustion and shorten the ignition delay.

$m_2$: needs to be calibrated to scale the calculated turbulent velocity $u_T$ in Eq. (3) thus the burning rate in Eq. (2). This parameter strongly influences the turbulent transfer of unburned mixture into the flame zone and thus the burning rate. Increasing this value will shorten the 10–90% combustion duration.

$m_3$: needs to be calibrated to scale the calculated value of Taylor micro-length scale ($l_M$ in Eq. (5)) and thus adjust the characteristic burning time $\tau_b$. Increasing this value will reduce the burning rate of mixture and delay the entire combustion process.

$m_4$: needs to be calibrated to scale the computed convective heat-transfer loss by Eq. (14). Increasing this value will increase the convective heat-transfer loss in the combustion process.

The modified SI engine combustion and heat-transfer sub-models were obtained by introducing $m_1$, $m_2$, $m_3$ and $m_4$ into the Eqs. (1) and (2). The modified combustion and heat-transfer sub-models have been listed in the column named 'Modified model' of Table 2.

For the modified model, *DEM*, $m_1$, $m_2$, $m_3$ and $m_4$ were all calibrated to various engine speeds and loads covering the entire

engine speed–load operating range. At each speed–load point, those parameters were carefully calibrated using experimental data to perform accurate prediction of the HRR and heat loss. As a result, the modified combustion and heat-transfer sub-models could ensure high enough prediction accuracy in the entire engine operating range.

### 2.3. Calibration results for the GT-Power models

The Atkinson cycle engine was operated over a wide range of speed–load conditions on an engine dynamometer test bench. The experimental data for throttle angle, IVC timing, EVO timing, AFR, SA and the corresponding engine output data at each speed–load point have been acquired.

The relevant parameters in the Woschni and SITurb sub-models were calibrated at each experimental engine speed–load point. Moreover, in fact, those model parameters vary with the speed and/or load. The smaller the selected intervals of the speed and torque are, the more accurate the interpolation between those points is. However, if the test interval is too small, the workload to run the test and calibrate the model parameters becomes too large to be acceptable. Therefore, the tradeoff between the prediction accuracy and workload is necessary.

The selected experimental points of the speed and torque for calibrating the GT-Power models are shown in Fig. 2. The torque points at each speed are determined from the WOT torque to 1.2 Nm. For example, the torque points at the speed of 1000 rpm are 119.8, 116.7, . . ., 2.3, 1.2 Nm, while the those at 4400 rpm are 152, 148,. . ., 2.3, 1.2 Nm.

Calibration procedure for the sub-model parameters is shown in Fig. 3. Brief descriptions of the calibration procedure are presented here:

1. Input experimental values of the operating variables (IVC timing, etc.) at a speed–load point to start the calibration process.
2. Set a proper value of parameter *DEM* for the speed–load point. Generally, as the load decreases, *DEM* value increases. According to our experiences, *DEM* value is usually in a range of 0.9–1.5.
3. Calibrate the parameter $m_3$ to initially match the curves of the simulated and experimental HRR. Especially, the start and end of the HRR curve should be basically matched in this step. The value of $m_3$ is usually in a range of 1.5–4.0. Then moderately calibrate the parameters $m_1$ and $m_2$ to match the HRR and cylinder pressure before 50% combustion timing and their peak values. The values of $m_1$ and $m_2$ are usually in a range of 0.5–1.8.
4. Examine if the cylinder pressure after 50% combustion timing are matched. If not, calibrate $m_4$ to match this section of cylinder pressure. Then, re-calibrate $m_1$ and $m_2$ to match the peak pressure and entire HRR again considering that the parameter $m_4$ also affect the HRR before 50% combustion timing and peak cylinder pressure.
5. After matching the HRR and cylinder pressure, the error between the simulated and experimental *BSFC* should be in the acceptable range. If not, you must go back to step 4 to continue calibrating $m_4$ and accordingly $m_1$ and $m_2$ to correct the predicted *BSFC*.
6. Repeat the steps 1–5 until the parameters of all speed–load points are calibrated.

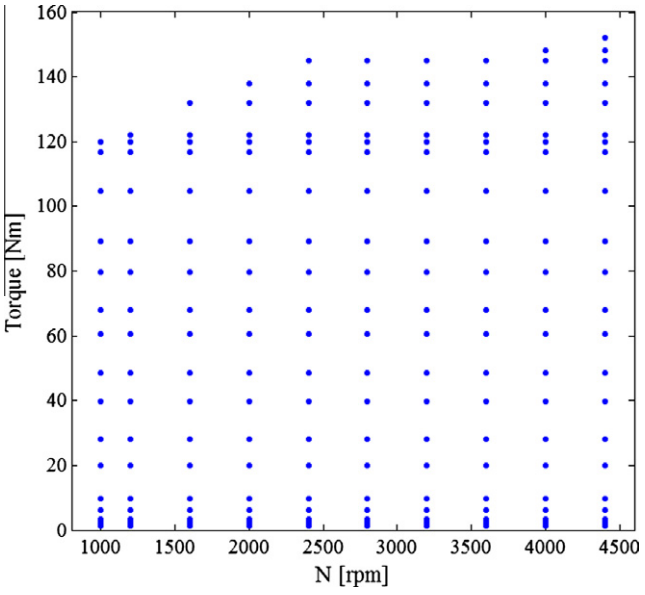


**Fig. 2.** Experimental points covering entire speed–load range.

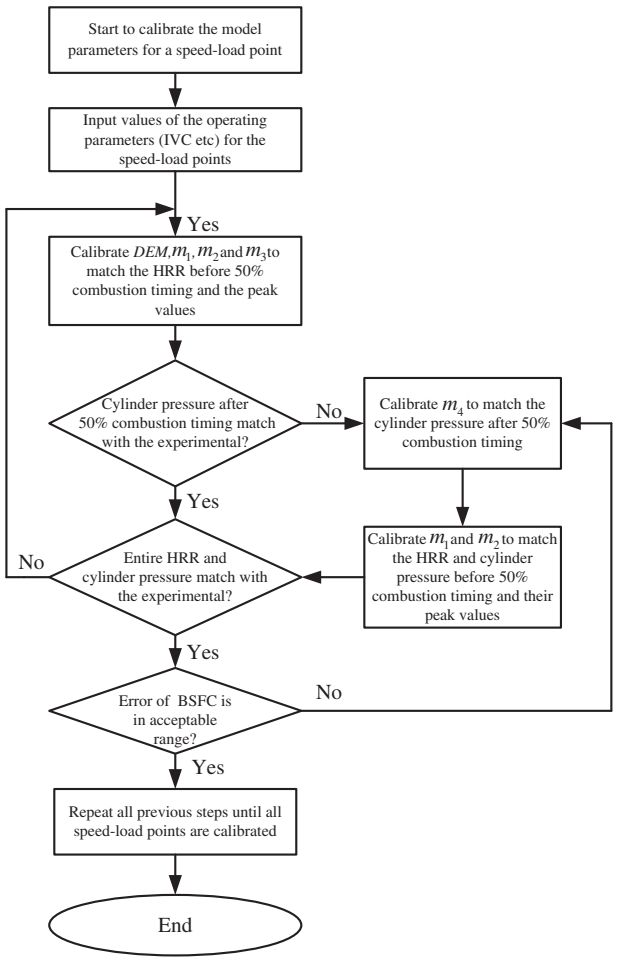


**Fig. 3.** Flowchart for calibrating the sub-model parameters.

Calibrations for the parameters of *DEM*, $m_1$, $m_2$, $m_3$ and $m_4$ are a process of trials and errors. There is not general experience to guide us to search for the optimum values of these parameters. Carefully and repeatedly combined calibrations for these parameters have to be manually done in order to accurately predict the HRR at each speed–load point. Once these model parameters are calibrated, they are not changed in the following GA optimization stage of the operating variables.

Figs. 4–6 show the comparisons of HRR between the predicted and measured results at speeds of 1000 rpm, 2800 rpm and

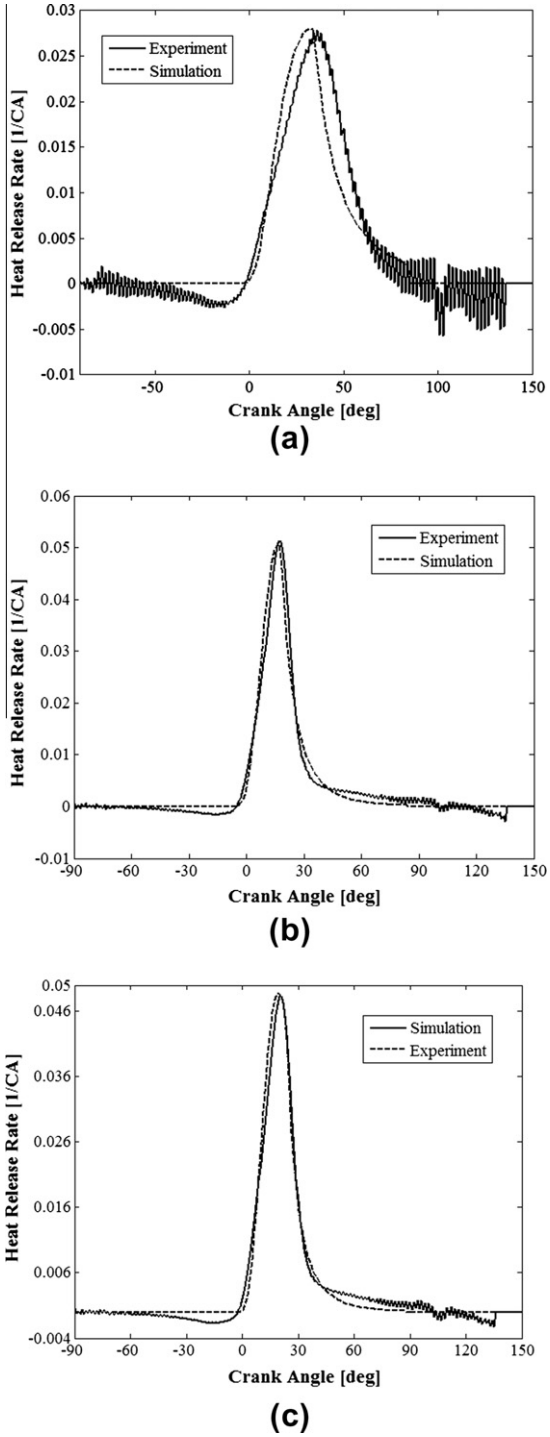


**Fig. 4.** HRR comparison for three load levels at 1000 rpm: 10 Nm, 90 Nm and WOT (119 Nm): (a) HRR at 10 Nm@1000 rpm, (b) HRR at 90 Nm@1000 rpm, (c) HRR at 119 Nm@1000 rpm.

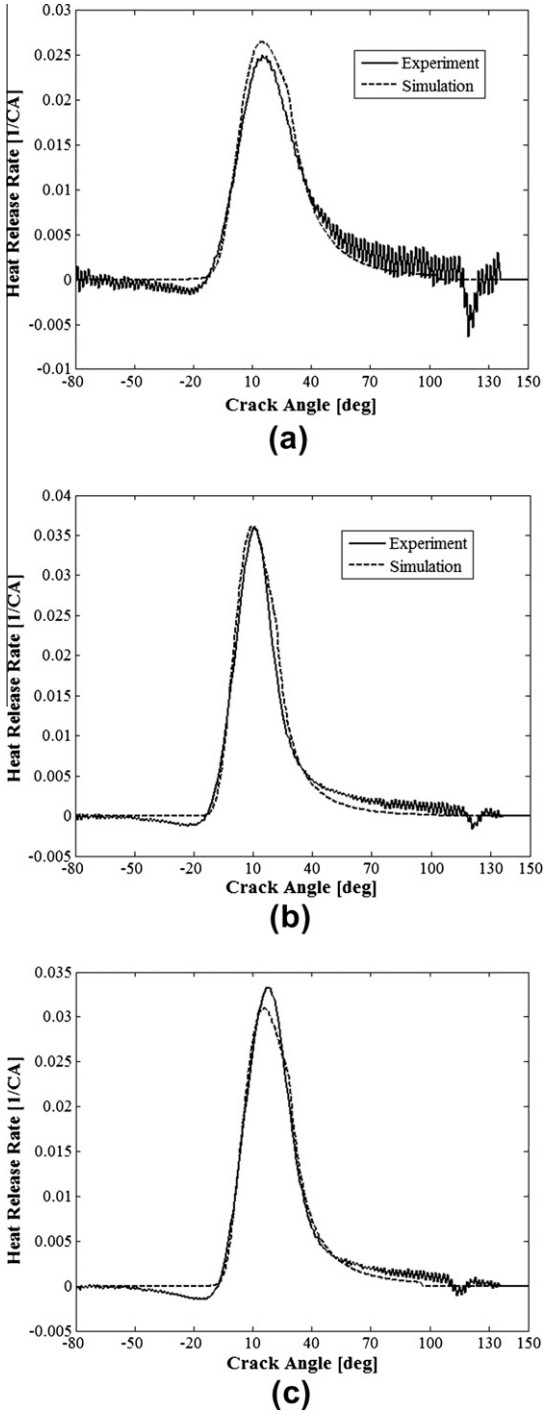


**Fig. 5.** HRR comparison for three load levels at 2800 rpm: 10 Nm, 90 Nm and WOT (145 Nm): (a) HRR at 10 Nm@2800 rpm, (b) HRR at 90 Nm@2800 rpm, (c) HRR at 145 Nm@2800 rpm.

4400 rpm, respectively. For each speed, the representative load points of 10 Nm, 90 Nm and WOT torque are selected to present the low, middle and full load conditions, respectively. The matrix of the speed and load points shown in Figs. 4–6 could demonstrate the entire speed and load range of interest.

Generally speaking, the simulated HRR match quite well with the experimental results. At the low torque level of 10 Nm, the HRR prediction errors are relatively larger for all three speeds. As the engine speed increases, the low torque prediction error tends to be reduced. Nevertheless, the error is still within the acceptable range.

Table 3 shows the relative errors between the predicted and experimental *BSFC* results. The maximum relative error of *BSFC* is 6.71%, occurred at the low load conditions. At most operating conditions, the simulation error of the GT-Power model for the *BSFC* are much lower than the maximum value. Therefore, this calibrated GT-Power model has enough prediction accuracy, hence can be safely used to optimize the engine operating variables for further improvement of the fuel economy.

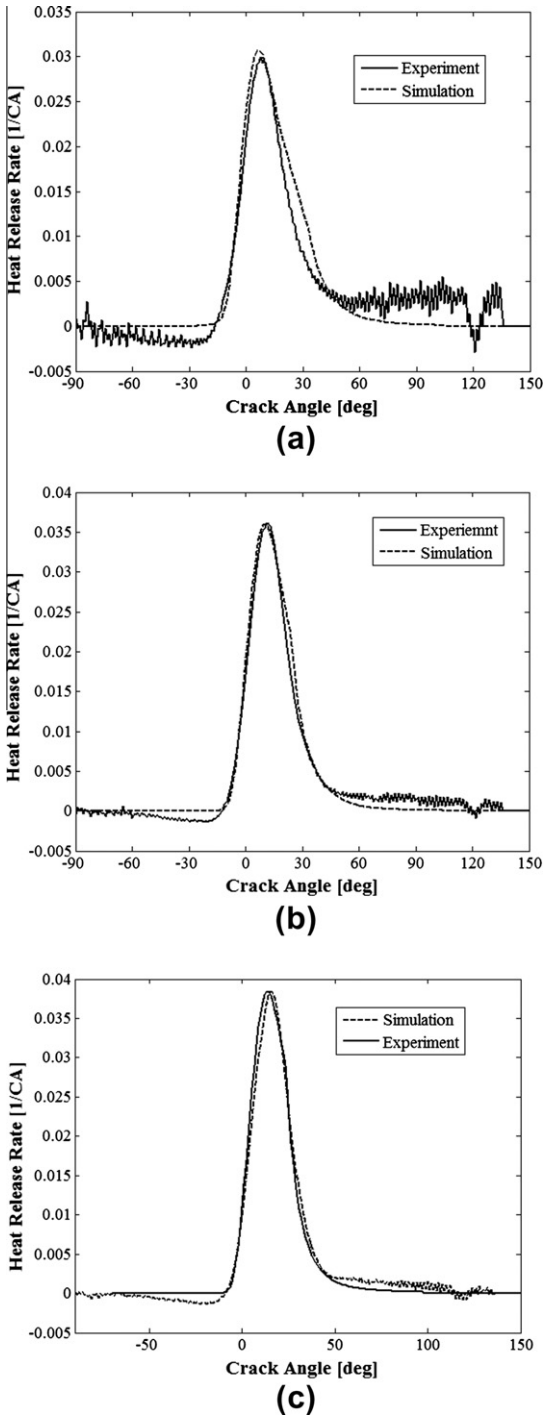


**Fig. 6.** HRR comparison for three load levels at 4400 rpm: 10 Nm, 90 Nm and WOT (152 Nm): (a) HRR at 10 Nm@4400 rpm, (b) HRR at 90 Nm@4400 rpm, (c) HRR at 152 Nm@4400 rpm.

If the knock restriction is not considered in the GT-Power simulations, it will make the optimization of the operating variables based on the models impractical. Thus, in order to optimize the operating variables with the consideration of knock restriction, the phenomenological empirical model for the knock index (KI) is used too [22]. The KI model used in the simulation was introduced in Ref. [1].

Temperature of the cylinder wall, piston crown and cylinder head mainly impacts the heat transfer loss and knock tendency. In the high to full load range, the knock tendency of the real engine is strong, thus in the model the temperature changes as the load changes. Above 70% load level, we make the temperature decrease as the load decreases. While in the middle to low load range, considering the knock tendency is slight we make the temperature constant in order to reduce the calibration workload. We only simply used $m_4$ to adjust the heat transfer loss in this operating range.

## 3. The model based GA optimization methodology

The introduction of the ETC valve has made it possible to use torque based engine control architecture [24–26]. The torque based control strategy increases the flexibility that manages the operating variables (such as the VVT timing), which make it possible to exploit the maximal potential of the actuators to improve the fuel economy.

The torque based control architecture is adopted in the Atkinson cycle engine. In order to be suitable for the torque based control architecture, the lookup tables, as function of speed and torque, for the ETC, IVC, EVO, AFR and SA need to be obtained in the calibration process of these operating variables.

In this section, a GA based optimization methodology is proposed and presented. The strategies that enhance the GA optimization efficiency are also investigated and validated. At last, the final optimization results of the five operating variables will be presented.

### 3.1. The genetic algorithm

For more than three decades, numerous attempts in imitating the living natural evolution process to solve the complex scientific and engineering system optimization problems have been tried and reported. Among them, the most popular evolutionary theory, genetic algorithm is inspired and developed [18,27].

The GA mimics the natural evolutionary process by introducing the principles of 'survival of the fittest' and genetics theory. The genetic information (gene) is stored in the chromosome and continuously evolves to better adapt the changing environment as the increasing generations. An individual in a population is corresponded with a chromosome. The individual in a population with best fitness has more probability to survive and to be selected for reproduction. In this way, the excellent gene in the individual is saved and strengthened. Goodness of an individual in any generation of the evolution process is indicated by defining a fitness function. Generally, the individual with smallest fitness function value is deemed the fittest member in a population [16–18,27].

There are two GA coded methods existing: binary and real coded. The average Euler distance between feasible solutions for the binary coded GA is less than that of the real number coded GA [28]. This means that the real number coded GA could better distribute the feasible solutions and find more real global optimum solution. Furthermore, it is also argued that a real number coded GA offers enhanced precision and more consistent results between different replications [16]. Therefore, genes of a chromosome are represented by real values within lower and upper bounds, and the float-point real number based crossover and mutation operation are adopted in this work.

For the Atkinson cycle engine, there are five optimization variables: ETC, IVC, EVO, AFR, and SA. The chromosome of each individual can be represented as a vector of five real values, where each real value represents a gene in the chromosome. The five real values are corresponded to the five operating variables, respectively. Therefore, each individual in a population represents a combination of the operating variables under the specific speed and torque. The fuel economy goodness corresponding to each individual is evaluated basing on the fitness function value. The crossover and mutation operation produce new children individuals based on

**Table 3**
The relative error of *BSFC*.

| N/torque | 1000 | 1200 | 1600 | 2000 | 2400 | 2800 | 3200 | 3600 | 4000 | 4400 |
|---|---|---|---|---|---|---|---|---|---|---|
| 152 | – | – | – | – | – | – | – | – | – | 3.16 |
| 148 | – | – | – | – | – | – | – | – | 3.25 | 2.21 |
| 145 | – | – | – | – | 1.38 | 0.45 | 1.08 | 1.43 | 2.76 | 1.79 |
| 138 | – | – | – | 2.23 | 2.43 | 1.59 | 2.39 | 1.69 | 2.68 | 2.48 |
| 132 | – | – | 1.67 | 1.78 | 1.99 | 2.58 | 2.91 | 3.29 | 1.29 | 3.29 |
| 122 | – | 2.9 | 2.67 | 1.99 | 2.67 | 3.24 | 1.59 | 2.49 | 3.29 | 1.93 |
| 119.8 | 2.23 | 2.54 | 2.58 | 2.45 | 1.74 | 3.45 | 4.39 | 3.17 | 4.23 | 2.59 |
| 116.7 | 1.89 | 2.56 | 3.27 | 2.75 | 2.45 | 3.51 | 2.84 | 1.29 | 3.92 | 3.29 |
| 104.7 | 2.56 | 1.78 | 2.58 | 3.47 | 2.58 | 2.49 | 3.76 | 3.21 | 2.69 | 4.23 |
| 89.3 | 3.56 | 4.78 | 3.18 | 1.89 | 1.94 | 0.28 | 2.36 | 2.59 | 3.49 | 1.27 |
| 79.5 | 2.98 | 3.97 | 1.84 | 0.68 | 2.87 | 1.94 | 2.49 | 0.75 | 1.17 | 0.92 |
| 68 | 1.78 | 2.89 | 3.78 | 3.12 | 2.19 | 2.97 | 3.43 | 3.59 | 2.29 | 3.25 |
| 60.4 | 1.57 | 3.24 | 2.67 | 2.19 | 3.28 | 4.18 | 3.21 | 2.78 | 3.23 | 2.68 |
| 48.4 | 2.34 | 2.87 | 1.96 | 3.68 | 2.97 | 3.29 | 2.58 | 4.57 | 2.29 | 3.14 |
| 39.7 | 3.93 | 1.85 | 2.89 | 3.97 | 3.16 | 1.49 | 2.18 | 5.23 | 1.48 | 4.68 |
| 28.2 | 2.52 | 4.76 | 2.53 | 4.37 | 1.49 | 2.79 | 3.48 | 3.15 | 4.12 | 3.71 |
| 19.8 | 2.79 | 3.28 | 3.57 | 2.59 | 3.14 | 2.69 | 4.9 | 2.39 | 2.94 | 2.58 |
| 9.8 | 1.69 | 4.73 | 2.69 | 3.65 | 2.79 | 3.8 | 5.3 | 4.28 | 3.33 | 4.29 |
| 6.3 | 2.67 | 3.45 | 4.73 | 3.78 | 3.64 | 2.28 | 2.58 | 3.65 | 4.34 | 6.16 |
| 3.5 | 2.45 | 3.89 | 5.25 | 4.82 | 3.15 | 4.89 | 5.29 | 4.32 | 5.49 | 4.39 |
| 2.3 | 3.78 | 5.12 | 4.78 | 2.38 | 4.32 | 6.71 | 6.25 | 5.77 | 3.59 | 5.49 |
| 1.2 | 4.32 | 5.89 | 6.34 | 5.27 | 3.69 | 5.36 | 4.68 | 6.49 | 5.59 | 4.72 |

the selected parent individuals in the reproduction pool. As the genetic generation increases, the sequential individuals gradually converge to the optimum individual with lowest fitness value.

After many trial and errors, it is found that the float-point coded *Heuristic Crossover* algorithm is more suitable for this optimization work. The child individual vector $Z$ generated by this algorithm is located on a line determined by two parent individual vectors $X$ and $Y$, as follows [29]:

$$Z = Y + r \times (X - Y) \tag{18}$$

where $X$ is the preferable individual vector, that is the fitness function $F(X) < F(Y)$ for minimization problems. $r$ is a random number lying in between 0 and 1, which is used to control the distance between the child individual $Z$ and the preferable individual $X$. The parent vectors, $X$ and $Y$, are randomly chosen individuals from the current reproduction pool.

Mutation operation could provide additional genetic diversity and it is thus more likely to avoid the local optimum solution. Mutation operations are performed according to some probability for the generated child vector by the crossover operations. The *Mutation Adaptable Feasible* algorithm can ensure that the variation for the five operating variables contained in the generated children individuals are always lying in the expectation bound, which can be depicted as follows [20]:

$$Z^{i+1} = r_1 \times Z^i + (1 - r_1)(r_2 \times (u - l) + l) \tag{19}$$

where $i$ indicates the generation number, and $r_1$, $r_2$ are independent, uniformly distributed random values generated from the range of (0,1), while $u$ and $l$ represents the upper and lower bound vector for the five operating variables, respectively.

### 3.2. The optimization scheme

Define vector $x$ = (ETC, IVC, EVO, SA, AFR) to represent a chromosome of an individual in the population, which means that each chromosome contains five genetic genes.

Optimizations for the operating variables were performed under the same speed–load points as those shown in Fig. 2. The GA based optimization scheme for maximizing the fuel economy of a given load point can be depicted as:

$$\text{Minimize} : BSFC(x, N) \tag{20}$$

$$\text{Subject to} : \text{Torque}(x, N) = \text{Torq}_{\text{obj}} \tag{21}$$

$$\text{IEGR}(x, N) < 22 \tag{22}$$

$$\text{KI}(x, N) < 200; \tag{23}$$

$$\text{Tem}(x, N) < 1150; \tag{24}$$

$$\text{Tem}(x, N) > 673 \tag{25}$$

$$1 \leqslant \text{ETC} \leqslant 90; \tag{26}$$

$$75\text{ABDC} \leqslant \text{IVC} \leqslant 115\text{ABDC} \tag{27}$$

$$90\text{ATDC} \leqslant \text{EVO} \leqslant 130\text{ATDC}; \tag{28}$$

$$-50 \leqslant \text{SA} \leqslant 0; \tag{29}$$

$$12.5 \leqslant \text{AFR} \leqslant 15.5; \tag{30}$$

where $BSFC(x, N)$ is the objective function of the GA optimization project; Eq. (1) is the equality restriction condition in order to maintain expectation load level; IEGR($x$, $N$), KI($x$, $N$), and Tem($x$, $N$) represents the percent in-cylinder combustion gas residual, knock intensity, and exhaust temperature before the TWC, respectively. Eqs. (22)–(25) are the nonlinear inequality restriction conditions of the GA optimization problem; and Eqs. (26)–(30) denote the variation range of the five optimization variables.

For the GA optimization problem with nonlinear restriction conditions, we need to translate the optimization with restrictions to the one without restrictions. Afterwards, the objective function of corresponding non-restriction GA optimization is just the fitness function of the initial GA optimization with nonlinear restrictions.

At present, there are many fitness function computation methods for the restriction optimization problem [28–30], including the simple static penalty function method and some dynamic penalty function methods, such as the Augmented Lagrange Barrier Algorithm [31]. Michalewicz and Schoenauer showed that the simple static penalty function method is more robust and efficient than those complex dynamic penalty function methods. Therefore, it is best practice to adopt the static penalty function method for most optimization projects [29].

In order to reduce the number of the penalty parameters and avoid being skewed to any restriction, all restriction conditions are normalized to make their absolute values less than one. Then all restriction conditions are multiplied by the same penalty parameter $R$.

Equality restriction condition Eq. (21) is normalized as:

$$\bar{h}(x) = \text{Torque}(x)/\text{Torq\_obj} - 1 \tag{31}$$

Inequality restriction conditions Eqs. (22)–(25) are normalized as:

$$\bar{g}_1(x) = \text{IEGR}(x)/22 - 1 < 0; \tag{32}$$

$$\bar{g}_2(x) = \text{KI}(x)/200 - 1 < 0; \tag{33}$$

$$\bar{g}_3(x) = \text{Tem}(x)/1150 - 1 < 0 \tag{34}$$

$$\bar{g}_4(x) = -\text{Tem}(x)/673 + 1 < 0 \tag{35}$$

Therefore, the fitness function for the GA based fuel economy optimization may be written as:

$$F(x) = BSFC(x) + R\left[\sum_{i=1}^{4} \max(\bar{g}_i(x), 0) + |\bar{h}(x)|\right] \tag{36}$$

The selection of the penalty parameter $R$ is very important for the GA optimization performance. If the $R$ value is too small, GA may search the optimum solution out of the feasible area and yield infeasible solution. Otherwise, if the $R$ value is too large, it may make the search of the real optimum solution rather difficult even impossible to find the real optimum solution. After many trials, the most appropriate $R$ value was determined as $10^3$.

The population size should increase as the complexity of optimization problem increases. The population size is generally selected according to empirical formula $(10/15) \times n$, where $n$ is the number of optimization variables. This optimization has five independent variables, and thus the population size is selected as 70. The crossover proportion is defined as: the proportion for the new individuals generated through the crossover algorithm in the next generation of population except the elite individuals. In this work, the crossover proportion is selected as 80%, while the maximum search generation number is 50 according to our practical experiences.

### 3.3. The model based GA optimization methodology

Fig. 7 shows the coupling scheme among the MATLAB (GA) program, Simulink model and GT-Power model. Fig. 8 shows the flowchart for GA based fuel economy optimization via the coupling of MATLAB/Simulink/GT-Power.

In order to enhance the GA efficiency for searching the global optimum solution, the GA fitness function values are computed in the vector formation. Therefore, after each generation of new population is produced, the GT-Power model is called to compute the objective function value and all restriction values for each individual until all individuals are finished. Then the fitness function value is calculated for the GA.

The work flow of the GA optimization under a given load point shown in the Figs. 7 and 8 could be described as:

1. The MATLAB program executes the GA to conduct the selection, crossover and mutation operation and produce new population;
2. the MATLAB program sets the corresponding values of the five optimization variables contained in an individual to the input module; then these values are transmitted to the GT-Power model via Simulink/GT-Power interface;
3. the GT-Power software performs the computation and returns required results (such as the torque) to the Simulink model via Simulink/GT-Power interfaceat real time;
4. the Stateflow module calculates the current computation cycle number of the GT-Power model based on the returned real-time crank angle by the GT-Power model;
5. the MATLAB program watches the current computation cycle number. When the cycle number is equal to 13, the MATLAB program collects the current values of the torque, *BSFC*, etc. and starts the calculation for the next individual;
6. repeat the steps 2–5 until all individuals in the current population are completely computed;
7. the MATLAB program computes the fitness function value using the returned results and produces a new population by implementing selection, crossover and mutation operations;
8. repeat the steps 1–7 until the stop criterions for the GA are met; then the optimum solution for the current optimization problem could be found.

The GA optimizes the operating variables of each speed–load point one by one until the optimization for all speed–load points are finished.

### 3.4. Strategy for accelerating the GA optimization

The SITurb and knock sub-models are adopted to predict the HRR and KI, respectively. The computation speed of the GT-Power model is much slower than that uses Wiebe function combustion model [22] without the knock model. As a result, if only one GT-Power model is participating in the individual computation at a time, the computation time for all individuals of each population is quite long. In our practice, when the population size and evolution generation number for the GA is set as 70 and 50, respectively, the optimization time for a load point at 4000 rpm is over 40 h! More than 98% time is spent by the GT-Power model to compute the fitness function values. Strategies for accelerating the computation are necessary.

As shown in Fig. 9, in order to accelerate the GA optimization on a computer with four CPU cores, we use four MATLAB to control four GT-Power models to collaboratively compute the individuals in a population at the same time. In Fig. 9, the top MATLAB executes GA while assigning computation tasks of individuals to the other three MATLABs. If there are more CPU cores in a single workstation, only need to increase the MATLAB-GT-Power group similar to that in Fig. 9.

However, the reduction in computation time is limited if only by adding new MATLAB-GT-Power computation groups in a single workstation computer. Fig. 10 presents the schematic for the distribution computation by linking multiple workstations via a local network. For any computer in Fig. 10, all CPU cores participate in the computation of the individuals similar to that shown in Fig. 9. The total computation time for the individuals could be greatly reduced.

On the other hand, as the evolution generation increases, the distance between the individuals in a new population becomes smaller and smaller. Therefore, the number of the individuals containing the same five independent variables increases. If these same individuals are all transmitted to the GT-Power model, there would be many repeated calculations. The following strategy was implemented: Once a population is produced, comparisons are performed among all individuals in this new population. For the same individuals, only one of them is preserved. Then, the preserved individuals are compared to those in the parent populations. If there are the same individuals, the corresponding GT-Power results saved in the previous data file are taken out and the relevant individuals in the new population are not computed again. At last, the all left individuals in the new population are divided into some parts and transmitted to the GT-Power model for new computations.

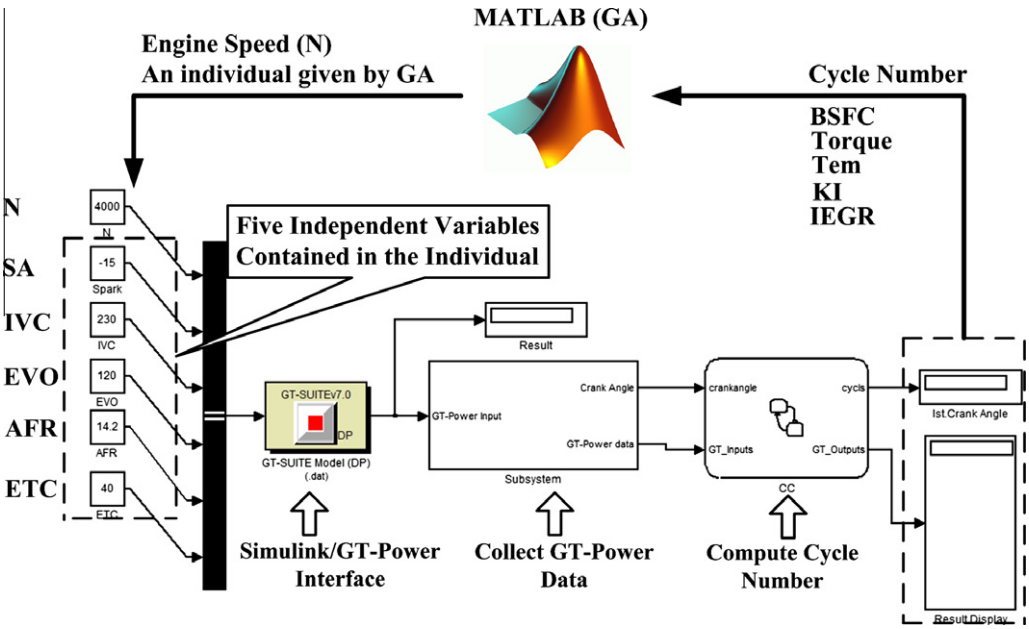


**Fig. 7.** MATLAB/Simulink/GT-Power coupling scheme.

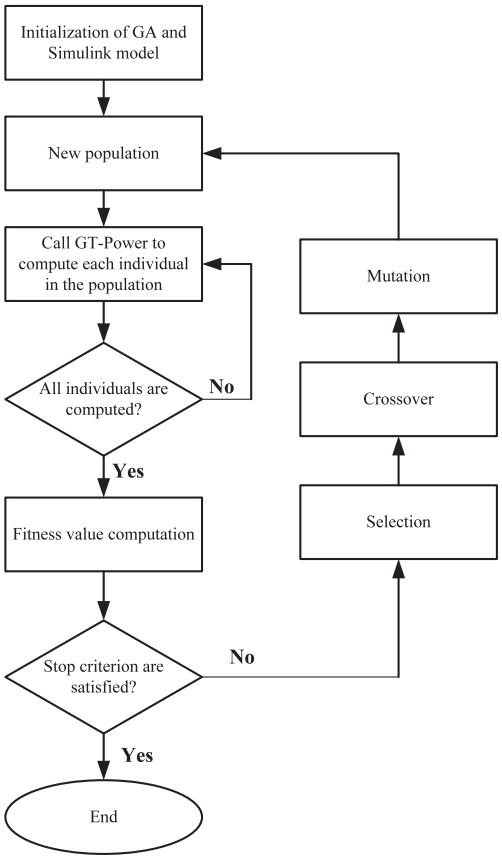


**Fig. 8.** Flowchart for fuel economy optimization via MATLAB(GA)/Simulink/GT-Power coupling.

### 3.5. Optimization results of the operating variables

Five HP xw6400 workstations were linked according to the strategies described in Section 3.4 to implement the fuel economy optimization based on MATLAB(GA)/Simulink/GT-Power coupling. Each xw6400 workstation has 4G memory and four CPU cores with

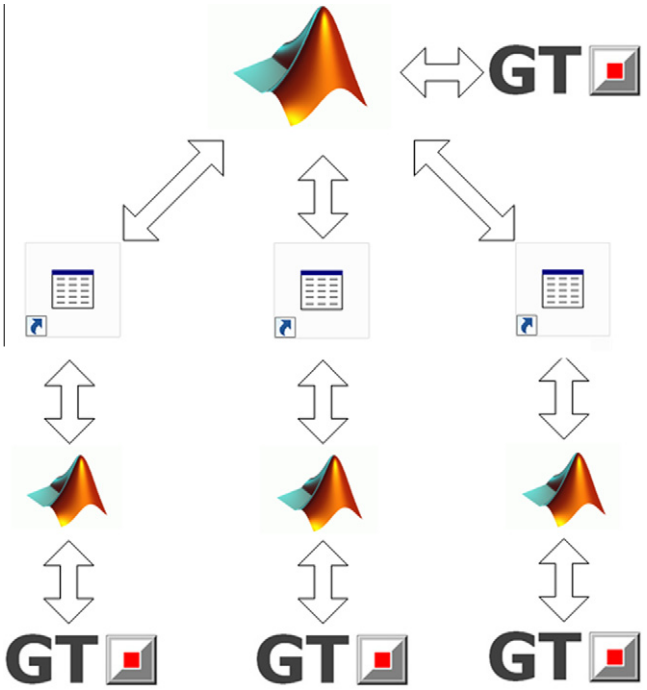


**Fig. 9.** Schematic for using multi-MATLABs to control multiple GT-Power models to compute the GA individuals.

their frequency of 2.0 GHz. The GA optimization speed was significantly increased. For example, for a load point at 4000 rpm, the time required for GA to run 50 generations was reduced to 5 h. Fig. 11 presents a typical GA evolution plot at 80 Nm torque and 4000 rpm. All GA solutions under all load points are feasible when the $R$ value is under $10^3$. Figs. 12–16 present the optimization results of the ETC, IVC, EVO, SA and AFR, respectively.

## 4. Experimental setup and method

The model based optimization results of the operating variables are only the reference points for the real experimental calibrations.

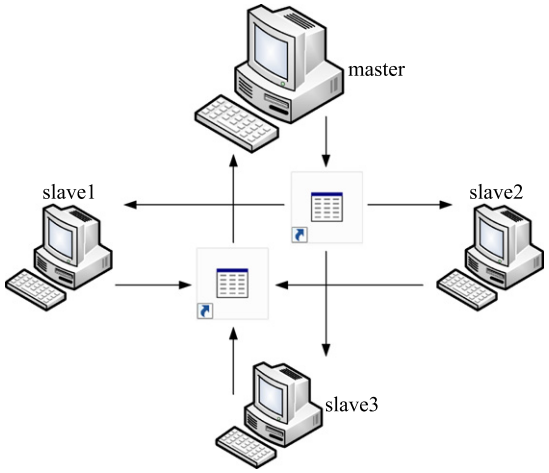


**Fig. 10.** Schematic showing the distributed computation based on multiple workstations.

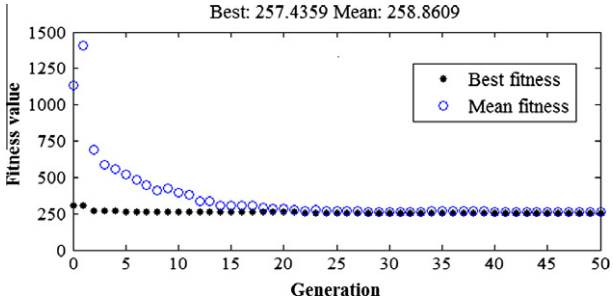


**Fig. 11.** GA evolution plot at 80 Nm torque and 4000 rpm.

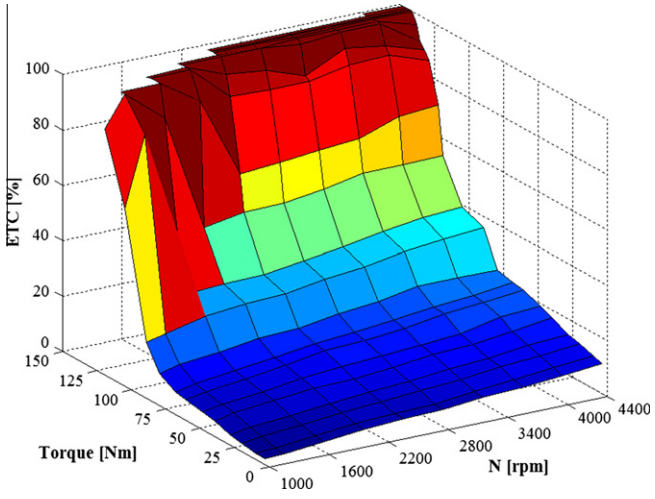


**Fig. 12.** Optimization results of ETC.

The differences between the simulated and the experimental results may exist. Therefore, the possible slight experimental adjustment of the optimized operating variables in Figs. 12–16 is necessary.

Fig. 17 presents the schematic of experimental setup. The AVL PUMA Control system performs the engine operation, collects and processes the engine performance data.

Each cylinder was installed a Kistler 6115AFD16 pressure transducer (0–200 bar) to capture the cylinder pressure data. The

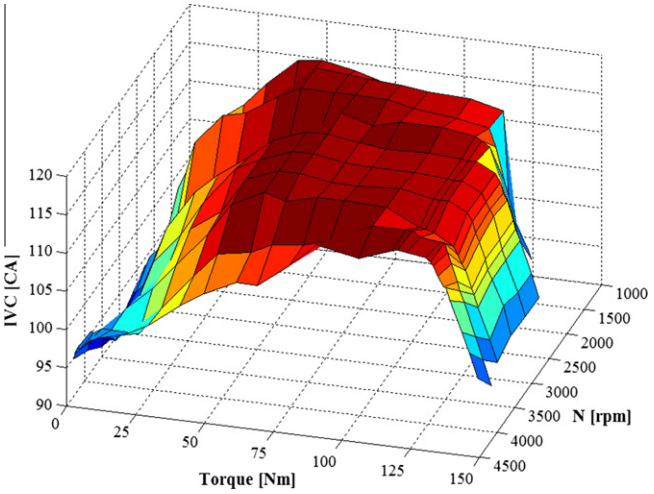


**Fig. 13.** Optimization results of IVC.

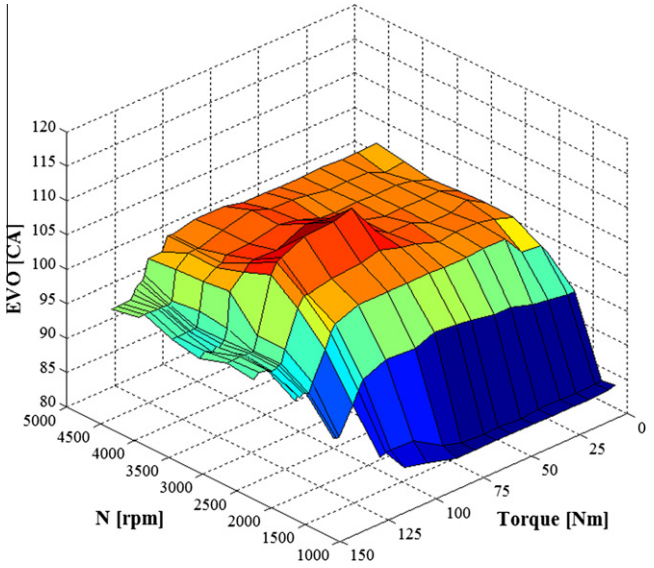


**Fig. 14.** Optimization results of EVO.

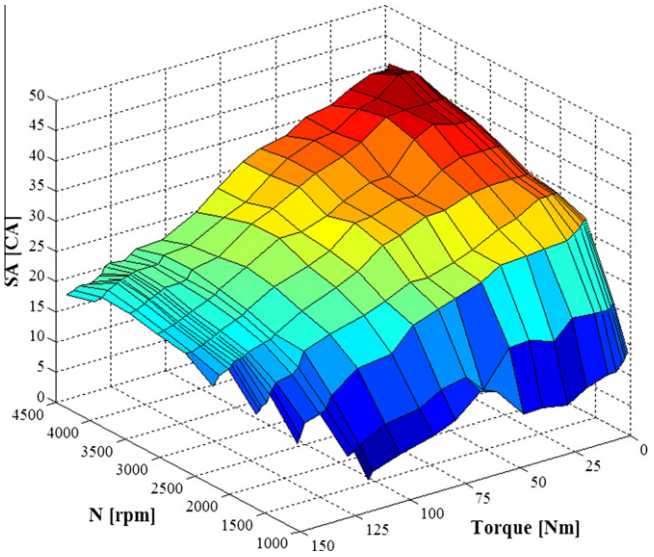


**Fig. 15.** Optimization results of SA.

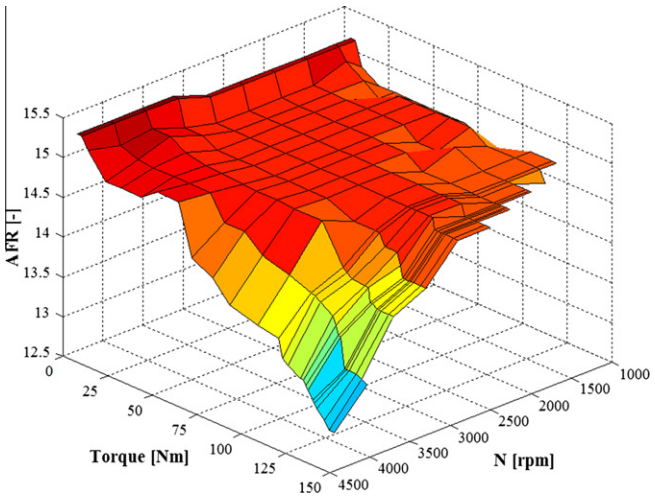


**Fig. 16.** Optimization results of AFR.

pressure data were conditioned using the Charge Amplifiers and then acquired by a high speed data acquisition system. The DEWETRON-800 combustion analyzer was used to process the pressure data and the digital encoder signal to evaluate the combustion performance and calculate the HRR.

A PT200 thermoelectric couple (−40 °C to +1000 °C) was installed upstream of the three-way catalyst convertor (TWC) to measure the exhaust temperature.

The AVL 330 kW AC dynamometer was connected to the engine to measure the torque. Maximum speed and measured torque accuracy of the dynamometer is 8000 rpm and 0.001%, respectively. The dynamometer was operated in speed-control mode to maintain the desired engine speed.

The AVL 733S fuel serving system and the AVL 733C fuel temperature control system provided accurate fuel mass data. The AVL 554/553 oil and coolant conditioning system maintained the engine oil and coolant temperature at 90 ± 1.5 °C.

The AVL Data Acquisition System collected all the engine data, including the charge temperature in the inlet port and exhaust temperature before the TWC.

The control maps of the five operating variables presented in Figs. 12–16 were embedded into the ECU via the ETAS-INCA system. Before the engine was cranked, all SAs in the SA map are retarded 5CA in order to avoid knock occurrence considering the possible difference between GT-Power model and real engine.

In the process of experimental calibration, at any engine load level, advanced the SA until the engine had slight knock, then retarded the SA until the knock disappeared. At the moment, the SA is determined the optimal value.

An ETAS-LA4 lambda analyzer was used to measure the $\lambda$ value of the exhaust gas before the TWC.

If the exhaust temperature is below 673 K, adjust AFR toward the stoichiometric value or retard SA until the exhaust temperature is above 673 K. If the exhaust temperature is above 1150 K, reduce the AFR from the stoichiometric value to enrich the mixture until the exhaust temperature is below 1150 K.

In every previous calibration process, adjusted the ETC opening to maintain the current torque at the target load level, and logged the *BSFC* at the same time.

## 5. Experimental results and discussion

The model based optimization results of the IVC and EVO timings were hardly modified in the experiment process while the SA, AFR and ETC results were slightly adjusted according to the experimental calibration methods in the Section 4. Comparison between the simulated *BSFC* and the measured ones is presented here to validate and demonstrate the prediction accuracy of the model.

Fig. 18 shows the relative errors between the simulated and experimental *BSFC* results. The *BSFC* for the simulated are the results computed under the optimized operating variables (Figs. 12–16) while the *BSFC* for the experimental are the measured values in the experiment process described in Section 4.

It can be concluded from Fig. 18 that the modified GT-Power model covering the entire speed–load range has sufficient

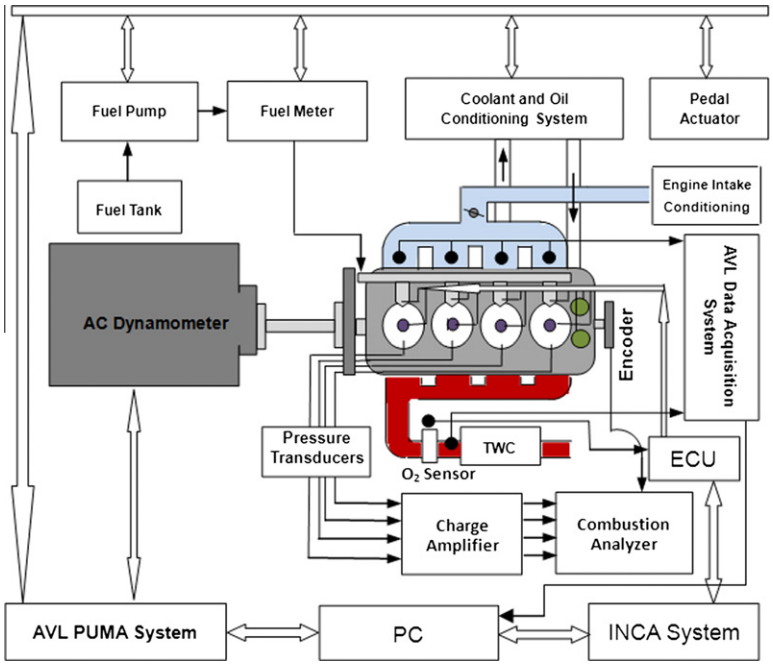


**Fig. 17.** Schematic of experimental setup.

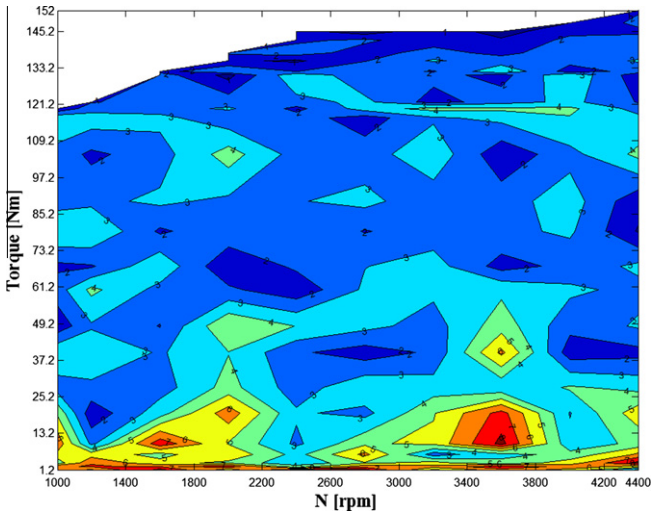


**Fig. 18.** Relative errors in percentage between the computed and experimental *BSFC* results.

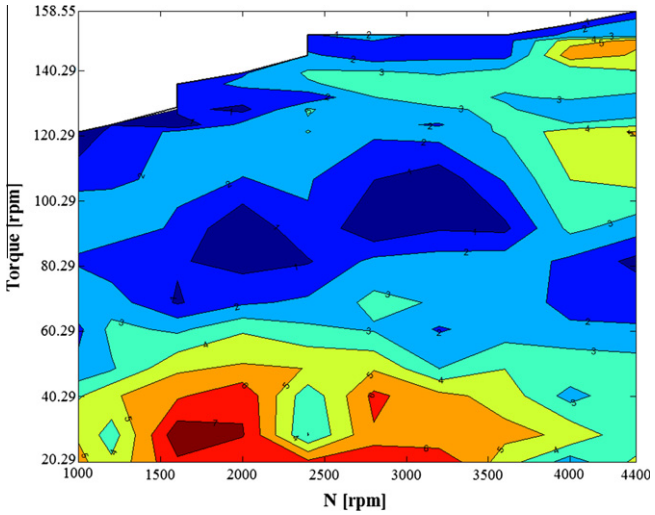


**Fig. 19.** Fuel economy improvement in percentage.

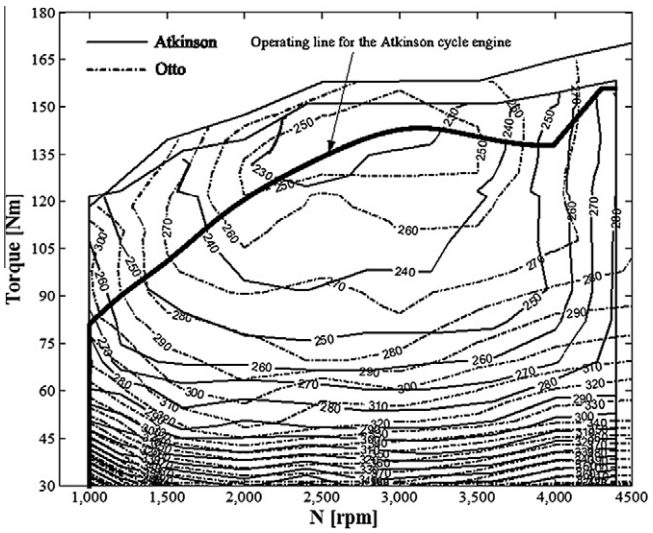


**Fig. 20.** Experimental *BSFC* comparison between the Otto and Atkinson cycle engines.

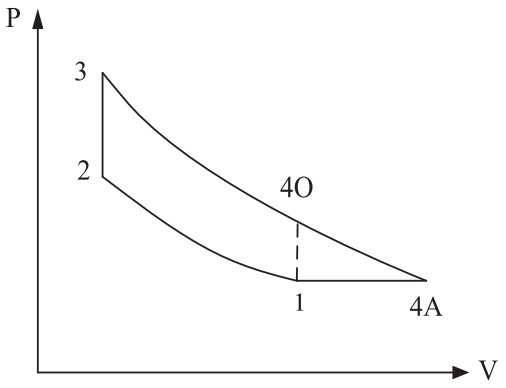


**Fig. 21.** *P–V* diagram of the basic Otto and Atkinson cycle.

prediction accuracy. The maximum error of the GT-Power model prediction after the GA optimizations comparing to the corresponding experimental results is 8.5%, occurring in the low load region. In the middle to high load region, the relative errors are relatively smaller, where the average error is about 3% with the maximal one as 4.5%. Therefore, it is acceptable to optimize the part load operating variables based on the modified GT-Power model.

Fig. 19 shows the *BSFC* improvement of the entire engine speed–load range. In the figure, the improvement percentage is defined as that the difference between the experimental *BSFC* before the GA optimization and the one after the GA optimization divides by the *BSFC* before the GA optimization. The experimental fuel consumption of the Atkinson cycle engine is obviously reduced after the GA optimization. It can be seen that the improvement levels are quite large in the regions of low loads, and high loads at high speeds. The maximal *BSFC* reduction is 7.67%, which is around the operating point of 28 Nm torque at 1600 rpm speed.

Fig. 20 shows the *BSFC* contour plots for the Otto and Atkinson cycle engines, respectively. It can be seen that the area of 250 g/kW h for the Atkinson cycle engine is greatly larger than that for the baseline Otto cycle engine. Moreover, the area of 240 g/kW h and 230 g/kW h for the Atkinson cycle engine is also very large while the corresponding area for the baseline Otto cycle engine is none. Therefore, in the medium to high load range, the Atkinson cycle engine has obviously higher fuel economy level comparing to the Otto cycle engine.

When the Atkinson cycle engine is used in a hybrid vehicle, great fuel economy improvement can be obtained if proper engine operating strategy is adopted. The most frequently used engine operating line in the hybrid vehicles has been plotted in Fig. 20. This engine operating line is realized by coordinating the work schedule of the engine and the electrical motor. In this way, the Atkinson cycle engine and the electrical motor can always work in their own most energy efficient region. For the engine, the idle operating conditions can be eliminated, and at most operating time the engine can always work in the region with relatively lower fuel consumption. Hence, the hybrid vehicle using the Atkinson cycle engine can achieve higher fuel economy level than the traditional vehicle with the Otto cycle engine.

## 6. Conclusions

The engine simulation model under various speed–load points covering the entire speed–load range of the Atkinson cycle engine was first built. Required experimental data were measured on an

engine test bench to accurately calibrate the model. The GA optimization methodology based on MATLAB(GA)/GT-Power coupling was developed for the part load fuel economy optimization. Then the strategies that could accelerate the GA optimization were proposed. Finally, the look up tables, as function of speed and torque, of the five operating variables were computed basing on the proposed methodology. Some conclusions for this work have been achieved:

(1) The modified GT-Power sub-models have sufficient prediction accuracy to simulate the part load engine performance and it can be used to optimize the operating parameters of the Atkinson cycle engine over the entire speed–load range.
(2) The automatic optimization scheme for the five operating variables of the Atkinson cycle engine has been realized by using genetic algorithm and MATLAB/GT-Power coupling, and the GA optimization efficiency is significantly improved due to the strategies developed in this work.
(3) The GA is effective in optimizing the engine operating variables to improve the fuel economy. After optimized by the GA, the fuel economy of the Atkinson cycle engine is improved up to 7.67%.
(4) Comparing to the baseline Otto cycle engine, the low fuel consumption area for the Atkinson cycle engine is significantly larger, which is beneficial for the fuel economy improvement of a hybrid vehicle adopting the Atkinson cycle engine.

## Appendix A

In 1882, an English engineer called James Atkinson designed the first Atkinson cycle engine. The engine can maintain normal compression ratio to avoid the knocking while implementing larger expansion ratio by the use of a clever mechanical linkages.

Fig. 21 shows the comparison of the *P–V* diagram of the Otto and Atkinson cycle. In the figure, 1-2-3-4O is the Otto cycle process while 1-2-3-4A-1 is the Atkinson cycle process. More heat energy (indicated as 4O-4A-1) can be converted into effective work output thus improving the thermal efficiency.

## References

[1] Zhao JX, Xu M, Li M, Wang B, Liu SZ. Design and optimization of an Atkinson cycle engine with the artificial neural network method. Appl Energy 2012;92:492–502.
[2] Nobuki K, Kiyoshi N, Toshihiro K. Development of new 1.8-l engine for hybrid vehicles. In: SAE technical paper no. 2009-01-1061; 2009.
[3] Katsuhiko H, Tatehito U, Toshifumi T, et al. The high-expansion-ratio gasoline engine for the hybrid passenger car. JSAE Rev 1999;20:13–21.
[4] Koichiro Muta, Makoto Yamazaki, Junji Tokieda. Development of new-generation hybrid system THS II – drastic improvement of power performance and fuel economy. In: SAE paper no. 2004-01-0064; 2004.
[5] Shiga S, Hirooka Y, Yagi S. Effects of over-expansion cycle in a spark-ignition engine using late-closing of intake valve and its thermodynamic considerision of the mechanism. Int J Automot Technol 2001;2(1):1–7.
[6] Fontana G, Galloni E. Variable valve timing for fuel economy improvement in a small spark-ignition engine. Appl Energy 2009;86:96–105.
[7] Osman AK, Hikmet A, Alper TC. Methods to improve efficiency of four stroke, spark ignition engines at part load. Energy Convers Manage 2005;46:3202–20.
[8] Anderson MK, Assanis DN, Filipi ZS. First and second law analyses of a naturally-aspirated, miller cycle, si engine with late intake valve closure. SAE technical paper no. 980889; 1998.
[9] Fukuzawa Y, Shimoda H, Kakuhma Y. Development of high efficiency miller cycle gas engine. Tech Rev 2001;38(3):146–50.
[10] Guerrier M, Cawsey P. The development of model based methodologies for gasoline IC engine calibration. In: SAE paper no. 2004-01-1466; 2004.
[11] Carter N, Gabler RA. Model based calibration process for robust optimal cam position selection under all engine operating conditions. In: SAE paper no. 2008-01-1366; 2008.
[12] Wu B, Prucka RG, Philipi ZS. Cam phasing optimization using artificial neural network as surrogate models-maximizing torque output. In: SAE technical paper no. 2005-01-3757; 2005.
[13] Wu B, Prucka RG, Philipi ZS. Cam phasing optimization using artificial neural network as surrogate models-fuel consumption and NOx emissions. In: SAE technical paper no. 2006-01-1512; 2006.
[14] Togun N, Baysec S. Prediction of torque and specific fuel consumption of a gasoline engine by using artificial neural networks. Appl Energy 2010;87:349–55.
[15] D'Errico G, Cerri T, Pertusi G. Multi-objective optimization of internal combustion engine by means of 1D fluid-dynamic models. Appl Energy 2011;88:767–77.
[16] Alonso JM, Alvarruiz F, Desantes JM, et al. Combining neural networks and genetic algorithms to predict and reduce diesel engine emissions. IEEE Trans Evol Comput 2007;11:46–55.
[17] Hiroyasu H, Miao H, et al. Genetic algorithms optimization of diesel engine emissions and fuel efficiency with air swirl, EGR, injection timing and multiple injections. In: SAE paper no. 2003-01-1853; 2003.
[18] Verma R, Lakshminarayanan PA. A case study on the application of a genetic algorithm for optimization of engine parameters. In: Proc. IMechE vol. 220 Part D: J automobile, engineering; 2006. p. 471–9.
[19] Vossoughi GR, Rezazadeh S. Optimization of the calibration for an internal combustion engine management system using multi-objective genetic algorithms. In: IEEE congress on, evolutionary computation; 2005. p. 1254–61.
[20] Lampinen J. Cam shape optimisation by genetic algorithm [J]. Comput Aided Des 2003;35:727–37.
[21] Li YG, Pilidis P. GA-based design-point performance adaptation and its comparison with ICM-based approach. Appl Energy January 2010;87(1):340–8.
[22] Gamma Technologies. Engine performance application manual. version 7.0; 2009.
[23] Heywood John B. Internal combustion engine fundamentals. McGraw-Hill; 1988.
[24] Heintz N, Mews M, Stier G, et al. An approach to torque-based engine management systems. In: SAE paper no. 2001-01-0269; 2001.
[25] Guénaël Le Solliec, Fabrice Le Berr and Gilles Corde, et al. Downsized SI engine control: a torque-based design from simulation to vehicle. In: SAE paper no. 2007-01-1506; 2007.
[26] Raymond Turin, Rong Zhang, Man-Feng Chang. Systematic model-based engine control design. In: SAE paper no. 2008-01-0994; 2008.
[27] Goldberg D. Genetic algorithms in search, optimization and machine learning. Reading, Massachusetts: Addison-Wesley; 1989.
[28] Deb Kalyanmoy. An efficient constraint handling method for genetic algorithms [J]. Comput Methods Appl Mech Eng 2000;186:311–38.
[29] Michalewicz Z, Schoenauer M. Evolutionary algorithms for constrained parameter optimization problems. Evol Comput 1996;4(1):1–32.
[30] Tsoulos Ioannis G. Solving constrained optimization problems using a novel genetic algorithm. Appl Math Comput 2009;208:273–83.
[31] Conn AR, Gould NIM, Toint Ph L. A globally convergent augmented Lagrangian barrier algorithm for optimization with general inequality constraints and simple bounds. Math Comput 1997;66(217):261–88.